H- and E-plane loaded Slow-wave structure for W-band TWT

Laxma R. Billa, M. Nadeem Akram, Claudio Paoloni and Xuyuan Chen

***Abstract*—Sheet beam vacuum electron tubes are an attractive solution for high-power sources or amplifiers at millimeter-waves. In this paper, a novel W-band slow-wave structure (SWS) for traveling wave tube (TWT) amplifier supporting a sheet beam is proposed. The SWS is based on a rectangular waveguide with H-plane and E-plane loaded metal corrugations. A test structure of the proposed H- and E-plane loaded (HEL) SWS with purposely designed input and output couplers was built in the frequency range of 91 – 98 GHz (W-band). The measured scattering-parameters agree well with the simulations showing S_{11}<-15 dB over 10 GHz bandwidth. A TWT was designed and simulated with the HEL SWS. It shows very good gain-bandwidth performance. The SWS is easy to manufacture by low-cost CNC-milling. The results demonstrated that the HEL SWS is a very good solution to build high-power, wideband millimeter-wave TWTs for a wide range of applications that need high power in a broad frequency range.**

***Index Terms*—Millimeter-wave, Traveling wave tube, Slow-wave structure, W-band Power Amplifier**

I. Introduction

Vacuum electronics is presently the only technology for high-power and wide-band signal sources and amplifiers operating at millimeter waves. The W-band (75 - 100 GHz) is of particular interest for radar systems and wireless communication systems for both terrestrial networks and satellite communications [1-5]. The rapid growth of solid-state transistor technologies, such as GaN, InP, has enabled the development of power amplifiers from microwave frequencies towards millimeter and sub-millimeter frequency ranges [6-7]. However, the solid-state device technology is limited to about 2 W RF power when the operating frequency approaches W-band. Beyond this frequency, the power reduces substantially. Vacuum electronic devices are able to provide tens of Watt power at millimeter waves. Travelling wave tubes (TWTs) in particular satisfy the system specifications for enabling many applications in the millimeter-wave frequency range and beyond [8-10].

A helix slow-wave structure (SWS) is not suitable for the frequency above 60 GHz due to the very small dimensions. TWTs at millimeter waves need all-metal SWS, that can support high-thermal loading, and must be vacuum compatible [10-11]. The folded waveguide has been widely used as SWS. It has been demonstrated in a number of TWTs in the millimeter-wave frequency range, such as Ka-band TWT [12-13], W-band TWT [14-15], D-band TWT [15], and G-band TWT [17]. The folded-waveguide SWS can be manufactured using CNC (Computer numerical controlled) milling up to G-band. However, it needs long machining time and requires complicated assembly [18]. The staggered double-vane SWS has been demonstrated for sheet-beam TWTs at the millimeter-wave [19]. The staggered double-vane SWS typically uses a high-aspect-ratio sheet beam that demands a relatively high value of an axial magnetic field to confine the modulated beam in its channel.

A novel SWS has been proposed, named the H-plane and E-plane loaded (HEL) SWS. It is suitable to be manufactured using low-cost CNC milling and offers high power and wideband operation. The performance of the TWT using HEL SWS has been investigated at 400-GHz frequency band [20]. The manufacturing feasibility of the SWS at this frequency band has been demonstrated by using LIGA process [21-22]. In this paper, the design, simulation and testing of a W-band TWT based on the HEL SWS is presented. Section II presents the design and electromagnetic simulation of the HEL SWS at W-band. The PIC (Particle-in-cell) simulation of a W-band TWT is discussed in section III. Section IV gives the manufacturing details and the scattering parameters (S-parameters) results of the HEL SWS.

II. H- and E-plane loaded SWS Design

A HEL SWS is devised by incorporating metal corrugations in both H-plane and E-plane of the rectangular waveguide, as shown in Fig. 1. The E-plane metal corrugation and the H-plane metal corrugation are loaded capacitively and inductively to the

This work was supported in part by the Ministry of Education, Norway, under the grant 02079, the Norwegian Micro- and Nano-fabrication facility NorFab (245963/F50).

M. Nadeem Akram, and Xuyuan Chen are with Department of Microsystems, University of South-Eastern Norway, Borre, Norway, 3184 (e-mail: muhammad.n.akram@usn.no; xuyuan.chen@usn .no).

Laxma R. Billa is with Department of Microsystems, University of South-Eastern Norway, Borre,Norway,3184 and with Engineering Department, Lancaster University, Lancaster, LA1 4YW, UK (e-mail:laxma.billa@usn.no and l.reddybilla@lancaster.ac.uk).

Claudio Paoloni is with Engineering Department, Lancaster University, Lancaster, LA1 4YW, UK (e-mail: c.paoloni@lancaster.ac.uk).

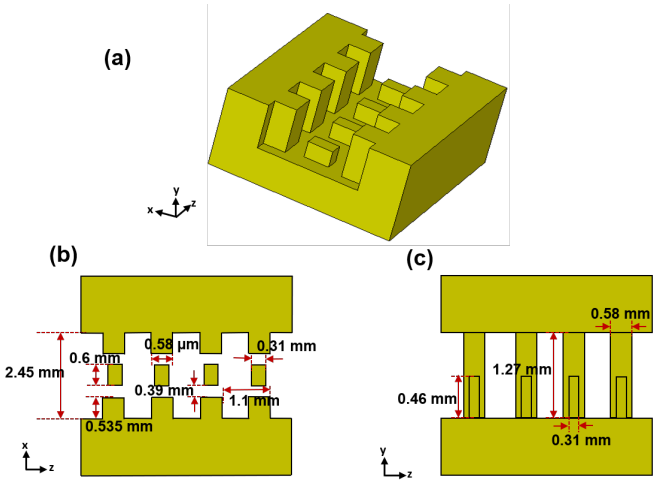

Fig. 1. Schmatic of the H-plane and E-plane loaded SWS: (a) 3 D view (remover top metal sheet), (b) top section view (excluding top metal sheet), and, (c) side section view (excluding sidewall).

electromagnetic field, respectively. The HEL SWS operates in the fundamental mode. Thus, the loading effects build the axial electric field, which allows the beam-wave interaction. Eigenmode simulations are performed by CST MWS. A unit period of the SWS is considered with periodic boundary conditions in the axial direction.

The parameters of the unit-cell structure are optimized to achieve a linear dispersion curve, at W-band, with a low beam voltage of ~20 kV. Importantly, the geometrical dimensions are also defined to ease the machining process by low-cost CNC tools.

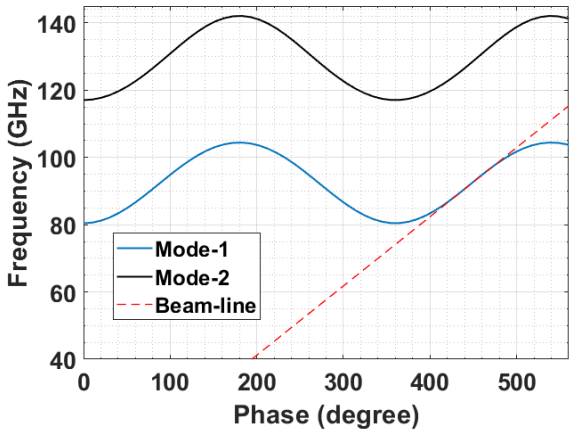

Fig. 2. Dispersion curve of the SWS.

The dispersion curve is shown in Fig. 2. The 20 kV beamline is superimposed to show the region of the electron beam velocity synchronized with the wave phase velocity. The dispersion curve is related to the first harmonics of the fundamental mode of the SWS, which covers the frequency range 80.4 – 104.2 GHz. The overlap of the beamline and the dispersion curve in the frequency range 87 - 99 GHz indicates a good synchronism condition for the wideband operation of the tube. The first higher-order mode is located in the band 117 - 142 GHz, showing a large bandgap which reduces the risk of band edge instability.

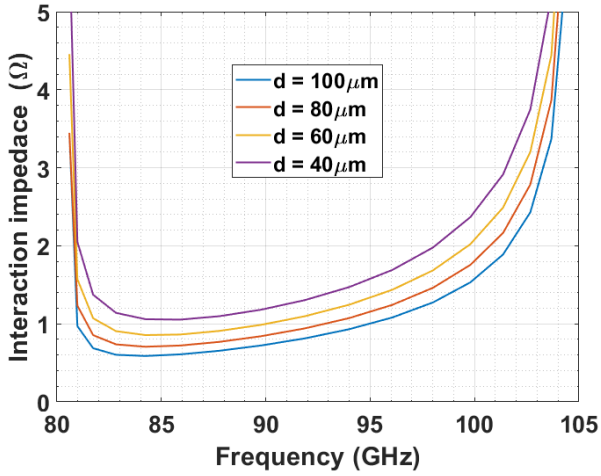

Fig. 3. Interaction impedance of the SWS for different positions of the beam with respect to the top of E-plane corrugations.

The Pierce interaction impedance is calculated using equation (1).

$$K_{cn} = \frac{\int_S \left| \frac{1}{P} \int_0^P E_z(x,y) e^{j\left(\frac{2\pi n}{P}\right)z} dz \right|^2 ds}{2\beta_n^2 P_{wg}} \quad (1)$$

Where, $P_{wg} = \frac{1}{2}\int dx \int \vec{E} \times \vec{H}\, dy$, $\beta_n = \beta_0 + {}^{2\pi n}/_{p}$, β_0 is phase constant, 'S' is beam cross-section assuming 1.0mm× 0.3mm that is positioned d distance above the top of the E-plane corrugation, E_z is the axial electric field, p is the unit period length of the SWS and n is the spatial harmonic number. The K_c is calculated using the field components and the dispersion curve obtained from Eigenmode simulations. The first space harmonic of axial electric field components of the forward wave (the phase shift between 360^0 to 540^0) is considered in the equation (1). Figure 3 shows the interaction impedance of the SWS for different values of d. If the beam is positioned closer to the edge of the E-plane corrugation, where the field is strong, a higher interaction impedance can be achieved. For $d = 80$ μm, the interaction impedance is more than 1 Ω over the desired operating bandwidth.

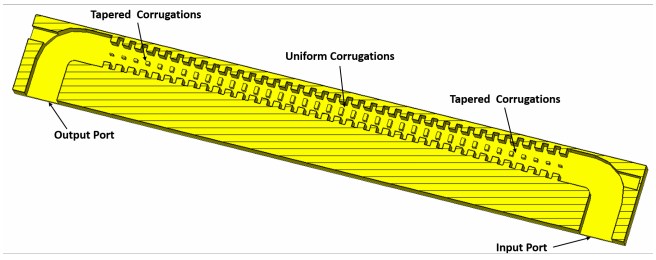

Fig. 4. Schematic of coupler design (top metal plate removoed).

A coupler is designed for a smooth wave transition from the rectangular waveguide TE_{10} mode to the slow-wave mode and vice versa. The coupler is composed of a finite length of waveguide section containing a tapered configuration of corrugations and a tapered waveguide width, as shown in Fig.

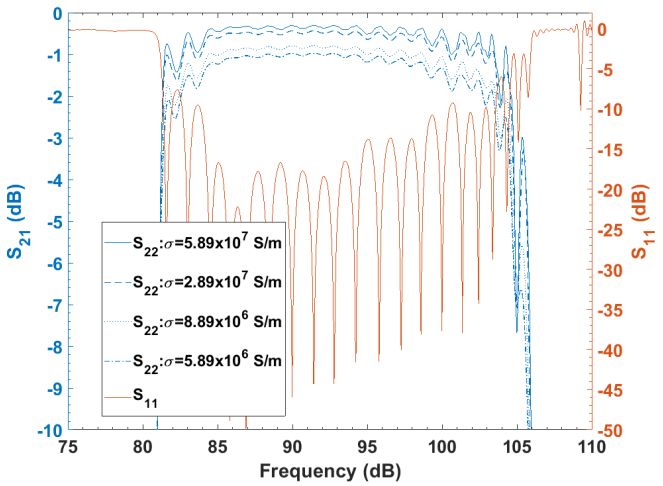

Fig. 5. S-paramters of the coupler design.

4. The width of E-plane corrugations in the coupler section is gradually narrowed towards the tail end of the SWS from the interaction section, while keeping other parameters of E-plane and H-plane corrugations unchanged. The change in the width of corrugation is of 60 µm. The time domain transient solver in CST MWS software is used to compute the S-parameters of the HEL-SWS with the coupler.

The simulation model includes ten uniform periods and nine tapered periods both at the input and the output (shown in fig. 4). The input and output ports are designed to match the WR-10 waveguide standard flanges. The coupler shows very good characteristics, S_{11}<-15 dB in the frequency range 84.5 - 98 GHz. A study of the effect of surface roughness on power loss is performed by simulating the HEL SWS with different values of conductivity of the OFHC (oxygen-free high thermal conductivity) copper. With a reduced conductivity, $\sigma = 0.598 \times 10^7$ S/m, the transmission loss of the SWS is about 1.3 dB and, 0.52 dB when the theoretical conductivity, $\sigma = 5.98 \times 10^7$ S/m, is considered, over the operating frequency.

III. W-BAND TWT DEMONSTRATION

The performance of the beam-wave interaction of W-band TWT based on HEL SWS is demonstrated by considering the interaction length with 85 periods. CST Particle Studio is used for the beam-wave interaction study. The optimized parameters derived from the Eigenmode simulations and transient simulations are used for the PIC simulations which include the interaction section, the input coupler, and the output coupler. The rectangular waveguide ports for the input and the output, the electron particle emitting surface, and the focusing magnetic field are also included. A reduced conductivity ($\sigma = 4.50 \times 10^7$ S/m) of OFHC copper is considered to account the surface roughness of the metal surfaces. A sinusoidal wave with 10 mW average power is used as an input signal. A uniform magnetic field of 0.9 T is applied for the electron beam focusing. The beam voltage is kept at about 21kV, and the beam current is set to 0.450 mA.

The initial cross-section dimensions of a rectangular sheet beam are b_w=1.00 mm and b_h=0.30 mm. It is positioned at a

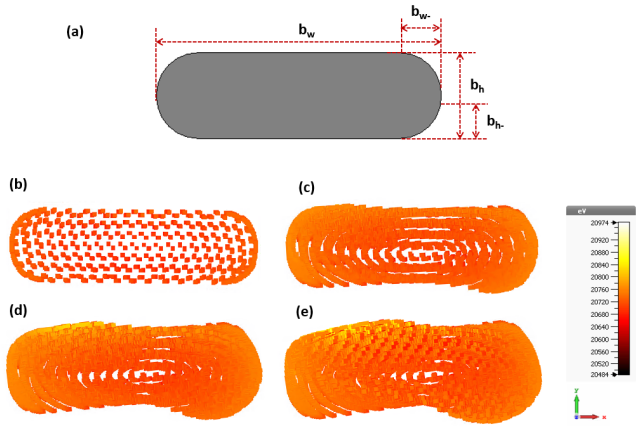

Fig. 6. (a) Schematic of modified beam cross-section from the rectangular-shaped sheet beam, and modulated sheet beam cross-section at different instance in the SWS:(b) 0 mm, (c) 30.8 mm, (d) 61.6 mm, and (e) 82.5 mm.

distance of d = 0.08 mm from the top of E-plane corrugations. It is found that the modulated sheet beam suffered from curling edges [23]. This curling edge is due to the $\vec{E} \times \vec{B}$ diocotron instability effect. The $\vec{E} \times \vec{B}$ force is always along the equipotential line, and the electron will drift following the equipotential line. To minimize the diocotron instability effects, the shape of the electron beam must match with the equipotential line. A modified rectangular cross-section with curved edges of the beam emitting surface is employed, b_{h-} = 0.14 mm and b_{w-}=0.14 mm (shown in Fig. 6(a)). Figure 6(b)-(e) show the cross-section of the modulated beam at different distance along the SWS length, during the beam-wave interaction process. The small-signal gain and output power of the 85-periods length TWT over the band is about 24 dB and 4.3 W respectively (Fig. 7). The gain of the TWT can be increased by using two or more sections of the SWS with severs or by implementing a velocity tapering technique.

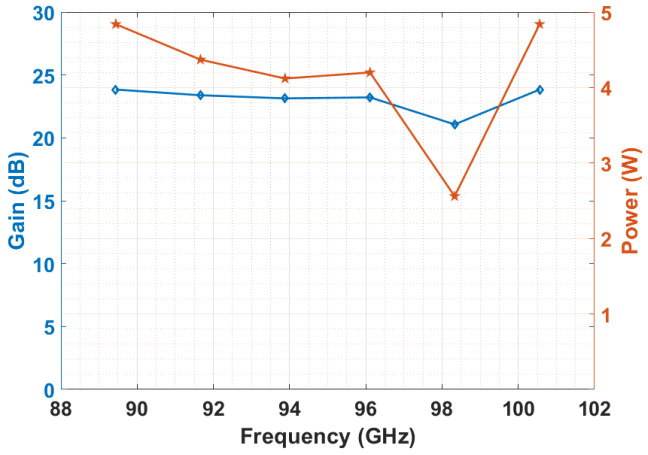

Fig. 7. Gain and Power of the TWT.

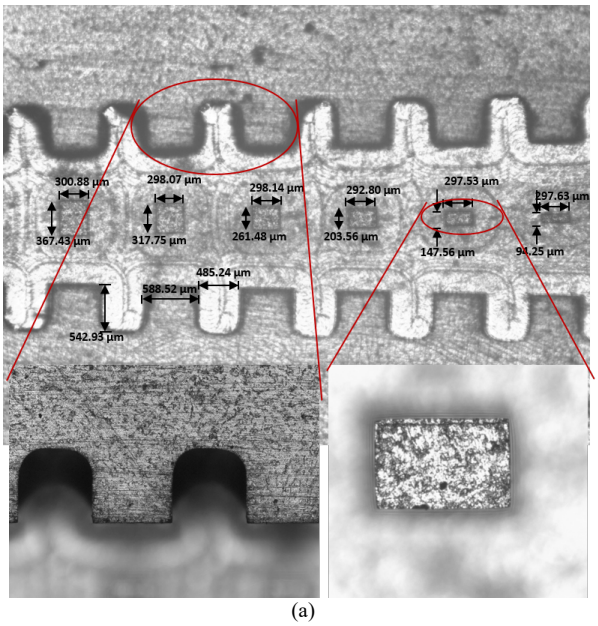

(a)

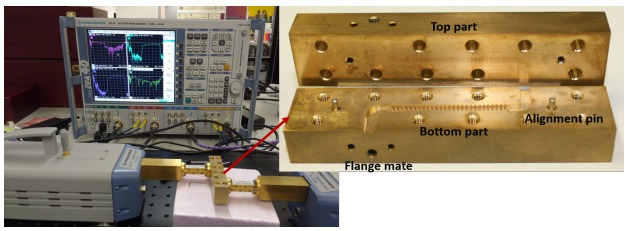

(b)

Fig. 8. (a) Optical microscopic images of the CNC-milled SWS, and (b) the SWS being tested under VNA.

IV. Manufacturing and Testing

The SWS was built into two parts, one with the corrugations and couplers, the other is a lid to close the waveguide. The two parts were assembled with nuts and bolts. As shown in Fig. 1, the size of the corrugations of the SWS is in the range of hundreds of microns (the E-plane corrugation with a minimum size has 0.09 × 0.31 mm in the tapered section). Manufacturing of such small parts using CNC milling needs a proper machining process. The tool diameter must be less than the size of the parts. An appropriate selection of the tools and optimized machining settings permits to obtain micro-level tolerance and sharp corners with good surface finish. The minimum distance between the parts to be machined is 390 µm. A tool with a 200 µm cutting diameter was used for machining those parts with 42000 rpm spindle speed.

For prototyping purpose, the HEL SWS was manufactured in copper alloy. The alloy is grade H62, which is composed of 63% copper, 0.15% Iron (Fe), 0.08% Lead (Pd), 0.005% Antimony (Sb), 0.002% Bismuth (Bi), and rest is Zinc. The CNC-milled SWS parts were ultrasonically cleaned with solvents to degreasing, and to remove organics residues and metallic debris from the milling process. The surface oxides were removed with acids. Optical microscopic images of the manufactured SWS parts are shown in Fig 8(a). The inner 90^0 corners were machined perfectly sharp, and tolerances are within 10 µm.

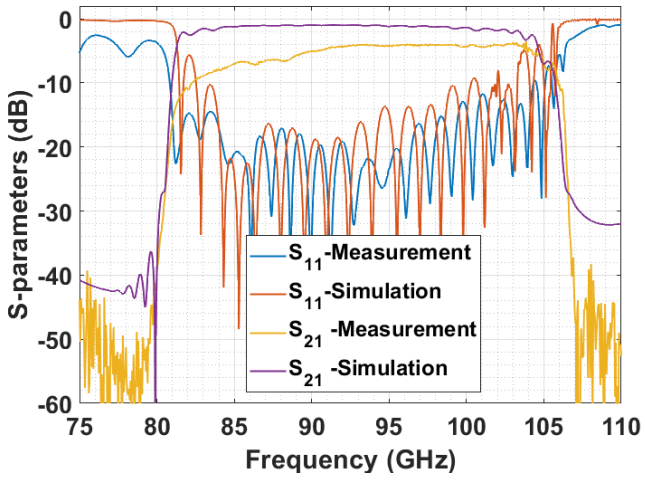

Fig. 9. Measured S-parameters of the CNC-machined SWS.

The S-parameters of the HEL SWS were measured using a Rhode & Schwarz vector network analyzer with W-band millimeter-wave extension modules. A good agreement between the simulation and the measurements was achieved, as shown the S-parameters in Fig. 9. A drift of ~2 GHz was presented at the lower and upper cutoff frequency. The reflection coefficient (S_{11}) was better than 15 dB and RF transmission loss in the SWS was measured about 4.5 dB over the operating bandwidth, 91 - 98 GHz. The higher transmission loss in comparison to the simulation (performed with a very low $\sigma = 0.598\times10^7$ S/m) was due to the imperfect metal surface finishing and the presence of tinny burrs and metal residues after cleaning. For future TWT hot-test experiments, the SWS will be manufactured with OFHC copper to improve the performance.

V. Conclusion

A novel SWS, H- and E-plane loaded waveguide, has been demonstrated as an effective solution for realizing millimeter-wave sheet beam TWT. The complete HEL SWS has been designed, manufactured, and validated by S-parameter measurements. The S-parameters measurements demonstrated broad bandwidth and low RF losses. The single section 85-periods HEL-SWS TWT provides 24 dB gain over 89 – 101 GHz. The promising performance of the HEL SWS demonstrates as suitable for producing an affordable and high performance millimeter-wave TWTs.

Acknowledgement

This project is supported by the Ministry of Education, Norway. The Research Council of Norway is acknowledged for the support to the Norwegian Micro- and Nano-fabrication facility, NorFab (245963/F50) and the Norwegian Ph.D. Network on Nanotechnology for Microsystems, Nano-Network (221860/F40).

REFERENCES

[1] Haynes, John M., Tristan S. L'Ecuyer, Graeme L. Stephens, Steven D. Miller, Cristian Mitrescu, Norman B. Wood, and Simone Tanelli. "Rainfall retrieval over the ocean with spaceborne W-band radar." *Journal of Geophysical Research: Atmospheres*, vol. 114, no. D8, 2009. doi: 10.1029/2008JD009973.

[2] Sassen, Kenneth, and Liang Liao. "Estimation of cloud content by W-band radar." *Journal of Applied Meteorology,* vol. 35, no. 6, pp.no. 932-938, 1996. doi: 10.1175/1520-0450.

[3] A. Jebril, M. Lucente, M. Ruggieri, and T. Rossi, "WAVE—A new satellite mission in W-band," in Proc. IEEE Aerospace Conference, Big Sky, MT, USA, Mar. 2005, pp. 870–879. doi: 10.1109/AERO.2005. 1559378.

[4] M. De Sanctis, E. Cianca, T. Rossi, C. Sacchi, L. Mucchi, and R. Prasad, "Waveform design solutions for EHF broadband satellite communications," *IEEE Commun. Mag.,* vol. 53, no. 3, pp. 18–23, Mar. 2015. doi: 10.1109/MCOM.2015.7060477.

[5] P. A. N. Ayllon, M. Ludwig, and R. Dionisio, "An overview of European space borne vacuum tube amplifiers and system needs," in *Proc. IEEE 18th Int. Vac. Electron. Conf.*, London, U.K., Apr. 2017, p. 12. Doi: 10.1109/IVEC.2017.8289697.

[6] Fung, A., Lorene Samoska, Pekka Kangaslahti, R. Lin, I. Mehdi, G. Sadowy, Simone Tanelli et al. "Gallium nitride amplifiers beyond W-band." In *2018 IEEE Radio and Wireless Symposium (RWS)*, pp. 150-153. IEEE, 2018. doi: 10.1109/RWS.2018.8304971.

[7] Tang, A., T. Reck, R. Shu, L. Samoska, Yangyho Kim, Y. Ye, Q. Gu et al. "A W-band 65nm CMOS/InP-hybrid radiometer & passive imager." In *2016 IEEE MTT-S International Microwave Symposium (IMS)*, pp. 1-3. IEEE, 2016. doi: 10.1109/MWSYM.2016.7540357.

[8] Dhillon,S.S., et al.,"The 2017 terahertz science and technology roadmap, " *Journal of Physics D*: Applied Physics, vol. 50, no.4, pp. 043001, 2017. doi: 10.1088/1361-6463/50/4/043001.

[9] Paoloni, Claudio, François Magne, Frédéric André, Xavier Begaud, Viktor Krozer, Marc Marilier, Antonio Ramirez, José Raimundo Ruiz Carrasco, Ruth Vilar, and Ralph Zimmerman. "Tweether future generation W-band backhaul and access network technology." In *2017 European Conference on Networks and Communications (EuCNC)*, pp. 1-5. IEEE, 2017. doi**:** 10.1109/EuCNC.2017.7980684.

[10] Basu, R., L. R. Billa, R. Letizia, and C. Paoloni. "Design of sub-THz traveling wave tubes for high data rate long range wireless links." Semiconductor Science and Technology 33, no. 12 (2018): 124009

[11] Paoloni, Claudio, et al. "Design and realization aspects of 1-THz cascade backward wave amplifier based on double corrugated waveguide." *IEEE Trans. on Electr. Dev.,* vol. 60, no. 3, pp. 1236-1243, Feb. 2013. doi: 10.1109/TED.2013.2240686.

[12] Booske, John H., Mark C. Converse, Carol L. Kory, Christine T. Chevalier, David A. Gallagher, Kenneth E. Kreischer, Vernon O. Heinen, and Sudeep Bhattacharjee. "Accurate parametric modeling of folded waveguide circuits for millimeter-wave traveling wave tubes." *IEEE Transactions on Electr. Dev., vol.* 52, no. 5 (2005): 685-694. Doi: 10.1109/TED.2005.845798.

[13] Han, Seong-Tae, K-H. Jang, Jin-Kyu So, Jung-Il Kim, Young-Min Shin, Nikita M. Ryskin, Suk-Sang Chang, and Gun-Sik Park. "Low-voltage operation of Ka-band folded waveguide traveling-wave tube." *IEEE transactions on plasma science, vol.* 32, no. 1 (2004): 60-66. doi: 10.1109/TPS.2004.823978.

[14] Hu, Yinfu, Jinjun Feng, Jun Cai, Xianping Wu, Yinghua Du, Jingkai Liu, Ji Chen, and Xiaoqing Zhang. "Design and experimental study of a wide bandwidth W-band folded waveguide continuous-wave TWT." *IEEE Transactions on Plasma Science, vol.* 42, no. 10, pp. 3380-3386, 2014. Doi: 10.1109/TPS.2014.2350477.

[15] Cai, Jun, Jinjun Feng, Yinfu Hu, Xianping Wu, Yinghua Du, and Jingkai Liu. "10 GHz bandwidth 100 watt W-band folded waveguide pulsed TWTs." *IEEE Microwave and Wireless Components Letters* 24, no. 9, pp. 620-621, 2014. Doi: 10.1109/LMWC.2014.2328891.

[16] Wenqiang, Lei, Jiang Yi, Zhou Quanfeng, Hu Peng, Hu Linlin, Yan Lei, and Chen Hong bin. "Development of D-band continuous-wave folded waveguide traveling-wave tube." In *2015 IEEE International Vacuum Electronics Conference (IVEC)*, pp. 1-3. IEEE, 2015. doi: 10.1109/IVEC.2015.7223857.

[17] Basten, M. A., J. C. Tucek, D. A. Gallagher, and K. E. Kreischer. "233 GHz high power amplifier development at Northrop Grumman." In *2016 IEEE International Vacuum Electronics Conference (IVEC)*, pp. 1-2. IEEE, 2016. doi: 10.1109/IVEC.2016.7561775.

[18] Gamzina, Diana, Logan G. Himes, Robert Barchfeld, Yuan Zheng, Branko K. Popovic, Claudio Paoloni, EunMi Choi, and Neville C. Luhmann, "Nano-CNC machining of sub-THz vacuum electron devices." *IEEE Trans. on Electr. Dev.,* vol. 63, no. 10, pp. 4067-4073, Aug. 2016. doi: 10.1109/TED.2016.2594027.

[19] Lai, Jianqiang, Yubin Gong, Xiong Xu, Yanyu Wei, Zhaoyun Duan, Wenxiang Wang, and Jinjun Feng. "W-band 1-kW staggered double-vane traveling-wave tube." *IEEE Trans. on Electr. Dev.,* vol. 59, no. 2, pp. 496-503, Aug. 2016. doi: 10.1109/TED.2011.2174458.

[20] Billa, Laxma R., M. Nadeem Akram, and Xuyuan Chen., "H-Plane and E-Plane Loaded Rectangular Slow-Wave Structure for Terahertz TWT Amplifier" *IEEE Trans. on Electr. Dev.,* vol. 63, no. 4, pp. 1722-1727, Apr. 2016. doi: 0.1109/TED.2016.2527824.

[21] Billa, Laxma R., Xianbao Shi, M. Nadeem Akram, and Xuyuan Chen, "Improved Design and Microfabrication of H -Plane and E -Plane Loaded Rectangular Slow-Wave Structure for THz TWT Amplifier," *IEEE Trans. on Elect. Dev.,* vol. 64, no. 5, pp. 2383-2389, May 2017. doi: 10.1109/TED.2017.2683399.

[22] Billa, Laxma R., Xianbao Shi, Muhammad Nadeem Akram, and Xuyuan Chen, "MEMS fabrication of H-plane and E-plane loaded 400 GHz TWT amplifier." In *2017 Eighteenth International Vacuum Electronics Conference(IVEC)*,pp.1-2.IEEE,2017.doi: 10.1109/IVEC.2017.8289683.

[23] Nguyen, Khanh T., John A. Pasour, Thomas M. Antonsen, Paul B. Larsen, John J. Petillo, and Baruch Levush. "Intense sheet electron beam transport in a uniform solenoidal magnetic field." *IEEE Transactions on Electron Devices* 56, no. 5 (2009): 744-752. doi: 10.1109/TED.2009.2015420.